한국해양공학회 2000년도 춘계학술대회 논문집 PP. 75~80

Large eddy simulation of turbulent boundary layer effects on stratified fluids in a rotating conical container.

SANG-KI LEE, JUN-HONG BAE, EYL-SEON HWANG AND M. SADASIVAM
Shipbuilding and Plant Research Institute, Samsung Heavy Industries, Koje 656-710, Korea

KEY WORDS: Large eddy simulation, Turbulent Ekman boundary layer, Stratified fluid, Rotating fluid

ABSTRACT: *We revisit the arrested Ekman boundary layer problem, using a fully non-linear numerical model with the subgrid dissipation modeled by the large eddy simulation method (LES). The main objective of this study is to find out whether the dynamic balance of the arrested Ekman boundary layer explained by MacCready and Rhines (1991) is valid for high Reynolds number. The model solution indicates that for high Reynolds number and low Richardson number flows, the density anomaly diffusion by near-wall turbulent action may become intense enough to homogenize completely the density structure within the boundary layer, in the direction perpendicular to the sloping wall. Then the buoyancy effect becomes negligible allowing a near-equilibrium Ekman boundray layer flow to persist for a long period.*

1. Introduction

A clarifier is an effective means to separate particles from the waste stream, and is one of the typical equipment of offshore platforms used for the first stage separation (or removal) of the slurry particles from the untreated sea water. Filtering and chemical treatment are with necessary preliminary process required to obtain demineralized water which is then used for many purposes during the platform operations. The clarifier is a sort of large cylinder-type container with an agitator at its center which rotates at low speed. The bottom wall is usually up-sloped away from the center, so that heavier slurry particles or fluids can slide into the center of the clarifier by gravity force. For the treatment of about 1,000 ton/hour of sea water, the typical size of the clarifier is about 20m in radius and 3.5m in height. The rotation speed of the agitator usually does not exceed 10 ~ 30 rpm.

Since the heavier slurry particles are to be settled down and trapped near the bottom of the clarifier, the bottom boundary layer plays an important role for the radial movement of the slurry particles. For rotating fluids, the radial transport due to the joint effect of viscosity and rotation is called Ekman transport. The amplitude of the Ekman transport depends on the rotation speed and kinematic viscosity of the fluid. The physical mechanism of the Ekman transport has been known for almost a century (Ekman, 1905). However, if the fluid is stratified and the bottom wall is sloped, which is exactly the case for the clarifier, the cross-slope Ekman transport introduces a density anomaly into the boundary layer. Due to this density anomaly near the wall, buoyancy is created which counterbalances the cross-slope flow motion. The buoyancy continues to built up until the Ekman boundary layer collapses creating a slippery boundary layer near the sloping wall. This complicated dynamics was first brought up and explained by Phillips et al., (1986), and it is sometimes called "arrested Ekman layer problem". Thorpe (1987) obtained a linear steady state solution of the arrested Ekman boundary layer problem. His solution is very unique in which the interior flow is not an external condition that can be imposed, but rather a part of the solution, since only a particular set of interior flow can be allowed to have a steady state solution. The physics of this peculiar solution is associated with the fact that the density anomaly induced by the Ekman transport must be dissipated or diffused away from the boundary layer, for a steady solution to exist. Therefore, in order to maintain the balance between the density anomaly dissipation and the buoyancy induced by the Ekman transport, the interior flow (which determines the strength of the Ekman transport) must be a function of the density diffusion coefficient.

MacCready and Rhines (1991) investigated the time dependent behavior of the arrested Ekman boundary layer problem. They found that, in the initial stage the Ekman transport induces strong buoyancy near the wall, and this buoyancy creates adverse pressure gradient which in turn decelerates the along-slope flow. Therefore, the Ekman transport must be also diminished. This deceleration process continues until the system achieves the Thorpe's steady state solution. The final state of their solution strongly depended on the density diffusion coefficient. If the density diffusion was not allowed, the final steady solution was a complete destruction of the interior flow field.

It is to be noted, however, there were a few restrictions in the arrested Ekman boundary layer models of Thorpe (1987) and

MacCready and Rhines (1991). For instance, the system of equations used was linearized version of the Navier-Stokes equations, the velocity component perpendicular to the bottom wall was assumed to vanish everywhere, and most importantly any flow variations in along-slope or cross-slope directions were not allowed. In this study we revisit the arrested Ekman boundary layer problem without imposing any restrictions, using fully non-linear numerical model. The main objective of this study is to find out whether the dynamic balance explained by MacCready and Rhines (1991) is valid for high Reynolds number. The model solution indicates that for high Reynolds number and low Richardson number flows, the density anomaly diffusion by near-wall turbulent action becomes so intense that the density structure within the boundary layer can be homogenized completely in the direction perpendicular to the sloping wall. Therefore, the buoyancy effects become negligible within the boundary layer allowing finite amplitude along-slope and cross-slope boundary layer flows.

In the following chapters, the physical problem is formulated, and the numerical solution is presented followed by a discussion on the physical implication of the model solution for boundary layer problems of rotating fluids.

2. Formulation of Problem

2.1 Governing Equations

The governing equations for the arrested Ekman boundary layer problem are obtained from equations of momentum, continuity and density for incompressible fluids in rotating reference frame. The Boussinesq approximation is used to account for the buoyancy effect. The equations are

$$\frac{\partial \boldsymbol{v}}{\partial t}+\boldsymbol{v}\cdot\nabla\boldsymbol{v}+2\boldsymbol{\Omega}\times\boldsymbol{v}=-\frac{1}{\rho_o}\nabla p-\frac{\rho}{\rho_o}\boldsymbol{g}+\nu\nabla^2\boldsymbol{v}, \tag{2.1}$$

$$\nabla\cdot\boldsymbol{v}=\boldsymbol{0}, \tag{2.2}$$

$$\frac{\partial \rho}{\partial t}+\nabla\cdot(\boldsymbol{v}\rho)=\nu\nabla^2\rho, \tag{2.3}$$

where the nomenclature is conventional: u and v are the cross-slope and along-slope velocities, ρ is the density, p is the pressure, ν is the kinematic viscosity, k is the density diffusion coefficient, is the acceleration of gravity and $\boldsymbol{\Omega}$ is the angular velocity of the reference frame. The density ρ is separated into three parts such that

$$\rho=\rho_o+\overline{\rho}(z)+\rho'(x,y,z,t). \tag{2.4}$$

To simplify the calculation procedure, the coordinate system is rotated by the angle of the wall slope θ as shown in Figure 1, then the equations (2.1) - (2.3) become:

$$\frac{Du_r}{Dt}-f\cos(\theta)(v_r-V_g)=-\frac{1}{\rho_o}\frac{\partial p'}{\partial x_r}-g\rho'\sin(\theta)+\nu\nabla_r^2u_r, \tag{2.5}$$

$$\frac{Dv_r}{Dt}-f\cos(\theta)u_r-f\sin(\theta)w_r=-\frac{1}{\rho_o}\frac{\partial p'}{\partial y_r}+\nu\nabla_r^2v_r, \tag{2.6}$$

$$\frac{Dw_r}{Dt}-f\sin(\theta)(v_r-V_g)=-\frac{1}{\rho_o}\frac{\partial p'}{\partial z_r}-g\rho'\cos(\theta)+\nu\nabla_r^2w_r, \tag{2.7}$$

$$\frac{D\rho'}{Dt}-\nabla_r\cdot(v_r\rho')=-\frac{gN^2}{\rho_o}\sin(\theta)u_r+k\nabla_r^2\rho, \tag{2.8}$$

where the subscript r represents the variables in rotated coordinate, $f(=2\Omega)$ is the Coriolis parameter and N is the buoyancy frequency given by

$$N^2=-\frac{g}{\rho_o}\frac{\partial\overline{\rho}}{\partial z}, \tag{2.9}$$

The pressure p is decomposed into two parts

$$p=\overline{p}(x_r,z_r)+p'(x,y,z,t), \tag{2.10}$$

and the mean pressure is taken to be hydrostatic:

$$\frac{\partial\overline{p}}{\partial z}=-g(\rho_o+\overline{\rho}). \tag{2.11}$$

The along-slope geostrophic velocity V_g is then given by

$$V_g=\frac{1}{f\rho_o}\frac{\partial\overline{p}}{\partial x}, \tag{2.12}$$

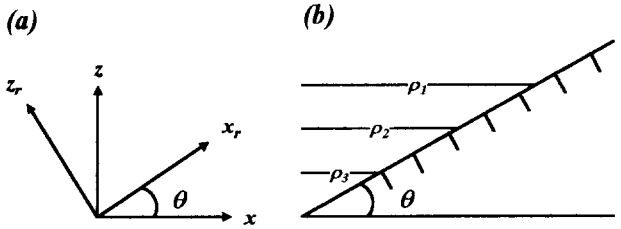

Figure 1. This figure shows (a) the rotated coordinate system and (b) initial stable stratification ($\rho_1 < \rho_2 < \rho_3$).

2.2 Boundary Conditions

The bottom boundary is no-slip and insulated:

$$u_r=v_r=w_r=0 \quad \text{at } z_r=0, \tag{2.13}$$

$$\frac{\partial\rho'}{\partial z_r}=\frac{gN^2}{\rho_o}\cos(\theta) \quad \text{at } z_r=0, \tag{2.14}$$

the top boundary is free-slip:

$$u_r = 0 \text{ as } z_r \to \infty, \tag{2.15}$$

$$v_r = V_g \text{ as } z_r \to \infty, \tag{2.16}$$

$$\rho' = 0 \text{ as } z_r \to \infty, \tag{2.17}$$

and the side boundaries are all periodic.

2.3 Dimensionless numbers

There are three important dimensionless numbers which are relevant to the current problem. They are Reynolds number, Richardson number and Prandtl number, which can be written as

$$Re = \frac{V_g \delta_E}{\nu}, \tag{2.18}$$

$$Ri = \frac{N^2 \delta_E^2}{V_g}, \tag{2.19}$$

$$Pr = \frac{\nu}{k}, \tag{2.20}$$

respectively, where δ_E is the laminar Ekman length given by

$$\delta_E = \sqrt{\frac{2\nu}{f\cos(\theta)}}. \tag{2.21}$$

It is to be noted that Pr is not an important parameter for turbulent flows since eddy diffusions (of momentum and density) are much intense than the molecular diffusions in the case of turbulent flows.

2.4 Numerical Method

The governing equations (2.5) - (2.8) are integrated using the FLUENT, a commercial CFD code developed by FLUENT INC (FLUENT, 1998). The finite volume method (FVM) is used for discretization of the governing equations, and mixed implicit - explicit scheme is used for time marching. A complete description on the numerical scheme of the FLUENT can be found in FLUENT manual (FLUENT, 1998).

The model domain size is $0.2m \times 0.2m \times 0.2m$ in, x_r, y_r and z_r directions, respectively. In order to resolve large eddies, if there is any, the grid size is set equal to the Ekman length in x_r and z_r directions. In vertical directions, there are 3 grid points within the Ekman length near the bottom wall, and the grid size increases away from the wall with the weighting factor of 1.2.

2.5 Large eddy simulation (LES) model

The Renormalization group (RNG) theory is used in order to account for the subgrid-scale eddy viscosity (Yakhot et al., 1989). The RNG procedure gives an effective subgrid viscosity μ_{eff}, given by

$$\mu_{eff} = \mu[1 + H(\frac{\mu_s^2 \mu_{eff}}{\mu^3} - C)]^{1/3}, \tag{2.22}$$

where

$$\mu_s = (C_{rng} V^{1/3})^2 \sqrt{2\bar{S}_{ij}\bar{S}_{ij}}, \tag{2.23}$$

and $H(z_r)$ is the Heaviside functions:

$$H(z_r) = \begin{cases} z_r, x_r > 0 \\ 0, \ x_r \le 0 \end{cases}, \tag{2.24}$$

and V is the volume of the computational cell. $\bar{S}_{ij}$ in 2.23 is the rate of strain tensor defined by

$$\bar{S}_{ij} \equiv \frac{1}{2}\left(\frac{\partial \bar{u}_i}{\partial x_j} + \frac{\partial \bar{u}_j}{\partial x_i}\right). \tag{2.25}$$

The theory gives C_{rng}=0.157 and C=100. A noble point of the RNG model compared with other LES models is in its ability to recover molecular viscosity in low Reynolds number regions. This fact makes the RNG scheme an excellent choice for the modeling the turbulent flows of their behavior not well investigated.

3. Results

3.1 Preliminary Experiment (case-1)

For neutrally stratified fluids, the Ekman layer becomes unstable at Re=55 (class A), and the secondary instability occurs at Re=110 (class B) (Greenspan, 1990). There are numerous literatures on the linear instability, transition to turbulence, and fully turbulent Ekman boundary layer solutions. However, for the arrested Ekman boundary layer problem, no theoretical analysis is available to determine in what conditions the flow becomes unstable and create large eddies, if any. The closest study relevant to the current problem may be the direct numerical simulation study of the stably stratified Ekman layer by Coleman et al., (1992). However, they considered only the flat bottom case, and since their focus was on the atmospheric boundary layer, the density value was fixed at the bottom, and the Prandtl number was that of the air which is an order of magnitude smaller than that of the water. Under these circumstances, they observed that, at the Reynolds number of 400, the Richardson number of 0.001 was near the maximum that allowed the flow to remain turbulent, and at this condition, the large coherent structures were not found. For neutrally stratified case, Coleman et al., (1990) extrapolated their DNS results for higher Reynolds number following the turbulent Ekman boundary layer theory developed by Csanady (1967).

Previous to Coleman et al., (1992), Mason and Derbyshire (1990) studied the stably stratified Ekman boundary layer with a LES model and obtained very similar results. Their success of the LES model partly supports our choice of the LES model for the simulation of the arrested Ekman boundary layer.

The model conditions for the preliminary simulation (case-1) are as follows: the reference density ρ_o is $1000 kg/m^3$, the buoyancy frequency N is $0.45 s^{-1}$, the slope angle θ is 10°, the kinematic viscosity ν is $10^{-6} m^2/s$ the thermal diffusivity k is $10^{-7} m^2 s$, the geostrophic velocity V_g is $-1 m/s$, the Coriolis parameter f is $1 s^{-1}$. The Ekman length δ_E is, using equation 2.21, $0.001425 m$, the Reynolds number Re is 1425, the Richardson number Ri is 4.06×10^{-7}, and the Prandtl number Pr is 10.

Figiure 2 shows the time history of the cross-slope transport at the center of the model domain. It is to be noted that the inertial oscillation emerges at the initial stage of the flow development, and it decays within several inertial periods $2\pi/f$. The arrested Ekman theories suggest that the cross-slope transport must decay exponentially to near zero, over a time scale of the shut-down time $f\cos(\theta)/(N\sin(\theta))^2$ (MacCready and Rhines, 1991). The shut-down time is the time it takes for the buoyancy effect to become important and the arrested Ekman boundary layer emerges. In this particular case, the shut-down time is about 29 seconds. However, as can be seen from the figure 2, after several periods of inertial oscillation the cross-slope transport becomes nearly constant. It is not obvious from this figure, but the cross-slope transport decays continuously at very slow rate.

Figure 3 illustrates the model solutions after 180 seconds of the model integration. The cross-slope velocity is relatively large, and the density is nearly homogenized within the boundary layer due to intense turbulent activities. It is to be noted that the wall boundary layer length is much thicker than that of the laminar Ekman boundary layer. More precisely, the turbulent boundary length δ_T can be estimated by u^*/f from dimensional analysis (Coleman et al., 1990). In this case, δ_E is $0.05 m$, which is about 35 times thicker than the laminar Ekman boundary layer length, indicating that turbulent motion plays much more significant role.

3.2 Influence of *Re* and *Ri* (case-2)

In order to understand the effect of different Reynolds number and Richardson number, the model simulation is carried out with much lower Reynolds number of about 142.5 and higher Richardson number of 4.06×10^{-6}. Figure 4 shows the time history of the non-dimensional spatial mean frictional velocity u^*/V_g at the bottom wall. Unlike the high Reynolds number case, the solution decays rather rapidly.

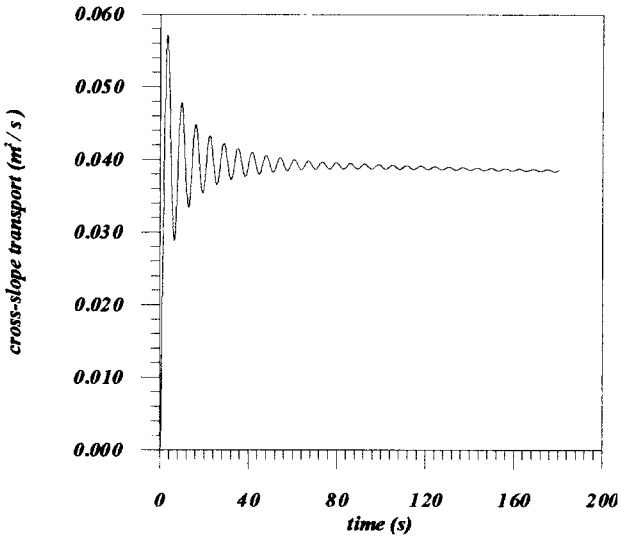

Figure 2. The time history of the cross-slope transport at the center of the model domain (case-1).

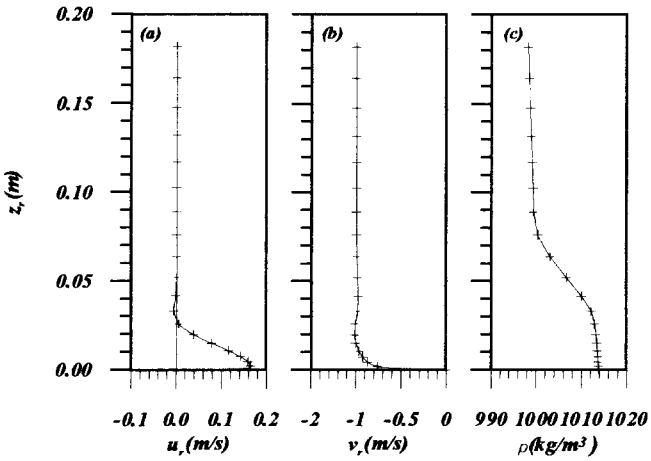

Figure 3. The model solutions (a) cross-slope velocity, (b) along-slope velocity and (c) density after 180 seconds of the model integration (case-1).

Figure 5, 6 and 7 shows the time variation of the model solutions u_r, v_r and ρ_r, respectively. The density anomaly slowly penetrates into the interior, which in turn creates adverse pressure gradient. Then the along-slope flow is decelerated by which the cross-slope flow is also decelerated. This flow pattern can be well explained by the arrested Ekman boundary layer theory of MacCready and Rhines (1991). It is, therefore, expected that the solution decays until it reaches the Thorpe's solution, if the system is integrated further in time.

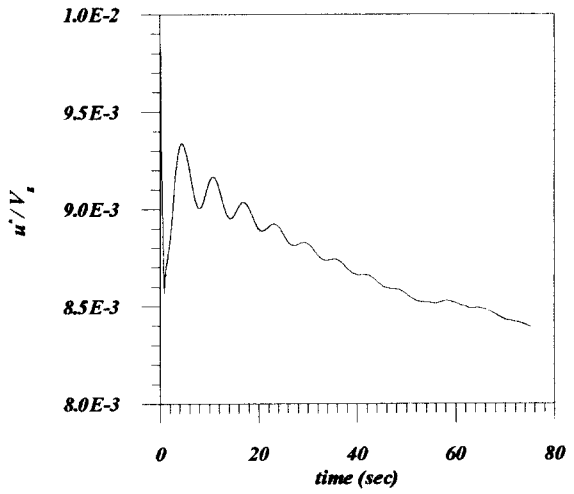

Figure 4. The time history of the non-dimensional spatial mean frictional velocity u^*/V_g at the bottom wall (case-2).

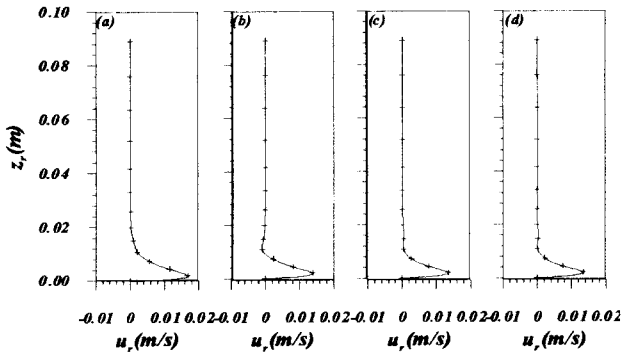

Figure 5. The time variation of the cross-slope velocity at (a) T=10sec (b) T=20sec, (c) T=50sec and (d) T=70sec, (case-2).

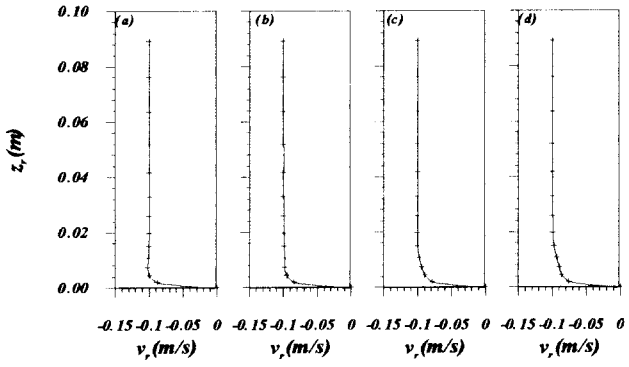

Figure 6. The time variation of the along-slope velocity at (a) T=10sec (b) T=20sec, (c) T=50sec and (d) T=70sec, (case-2)

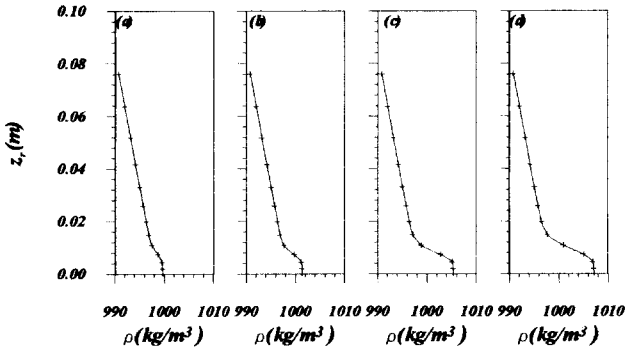

Figure 7. The time variation of the density at (a) T=10sec (b) T=20sec, (c) T=50sec and (d) T=70sec, (case-2).

4. Discussion

A series of large eddy simulations (LES) of the arrested Ekman boundary layer has been conducted. The major finding is that the behavior of the arrested Ekman boundary layer solution depends critically on both the Reynolds number and Richardson number. For the high Reynolds number and low Richardson number case, the wall boundary layer was characterized by fully turbulent small scale motions, and the boundary layer flow system achieved a finite amplitude near-equilibrium state. This model result is appears to be different from the conventional arrested Ekman boundary layer theory (MacCready and Rhines, 1991). The resolution is that, in this particular case, the near-wall density anomaly induced by cross-slope Ekman transport was diffused quickly within the boundary layer by intense turbulent motions. Since the density was nearly homogenized within the boundary layer, the buoyancy played no roles there. Therefore, the cross-slope Ekman transport (as well as the along-slope transport) persisted for a long period. The buoyancy played an important role only at the top of the boundary layer, by which the along-slope flow was decelerated continuously there. Although it is not obvious from the analyzed model results, we suspect that the turbulent density dissipation also played a non-negligible role for slowing down the density anomaly diffusion into the interior. This argument is in line with the eddy diffusion model of Garrett (1990). He derived a steady state solution for a given arbitrary interior velocity by choosing appropriate eddy diffusion coefficients. His steady state solution describes the dynamic balance between the continuous creation of buoyancy by cross-slope Ekman transport and its destruction by eddy dissipation process.

For low Reynolds number and high Richardson number case, the flow system decayed continuously, in accordance with the arrested Ekman boundary layer theory. We argue that, in this case, the turbulence density diffusion effect was not intense

enough to homogenize the density structure within the boundary layer. Therefore, the buoyancy played a significant role there, which in turn created adverse pressure gradient counterbalancing the boundary layer flows. The result is continuous decay of the boundary layer solution.

The upshot is that it is the relative magnitude of the Reynolds number and Richardson number that determines whether the flow system may or may not follow the arrested Ekman boundary layer theory. More precisely, if the turbulent intensity (which is determined by Reynolds number) is strong enough to homogenize completely the density structure (which is related to Richardson number) within the boundary layer, the flow system may achieve a near-equilibrium solution. Otherwise, the arrested Ekman boundary layer mechanism emerges, therefore the flow field decays continuously until it reaches the steady state restricted by Thorpe's solution.

The implication of these model results is important for the understanding of the bottom boundary layer of rotating equipment such as the clarifier. However, with proper choices of *Re* and *Ri*, same principles can be applied to the planetary boundary layers of atmosphere and oceans.

Acknowledgements

This work was supported by the Korean ministry of science and technology, 1999 specialized engineering R&D project, through a grant entitled "Development of engineering package for a barge mounted seabed sludge treatment plant".

References

Coleman, G. N., J. H. Ferziger and P. R. Spalart, 1990. A numerical study of the turbulent Ekman layer. J. Fluid. Mech., 213, 313-348.

Coleman, G. N., J. H. Ferziger and P. R. Spalart, 1992. Direct simulation of the stably stratified turbulent Ekman layer. J. Fluid. Mech., 244, 677-712.

Csanady, G. T., 1967. On the 'resistance law' of a turbulent Ekman layer. J. Atmos. Sci., 24, 467-471.

Ekman, V. M., 1905. On the influence of the earth's rotation on ocean-currents. Ark. Mat. Astr. Fys. 2, 1-52.

Fluent, 1998. FLUENT 5 User's guide Volume 2, Fluent Inc., Lebanon.

Garrett, C., 1990. The role of secondary circulation in boundary mixing. J. Geophys. Res., 95, 3181-3188.

MacCready, P., and P. B. Rhines, 1991. Buoyant inhibition of Ekman transport on a slope and its effect on stratified spin-up. J. Fluid Mech., 223, 631-661.

Mason, P. J., and S. H. Derbyshire, 1990. Large eddy simulation of the stably-stratified atmospheric boundary layer. Boundary Layer Met., 53, 117-162.

Phillips, O. M., J.-H. Shyu and H. Salmun, 1986. An experiment on boundary mixing: mean circulation and transport rates. J. Fluid Mech., 173, 473-499.

Thorpe, S. A., 1987. Current and temperature variability on the continental slope. Phil. Trans. R. Soc. Lond., A323, 471-517.

Yathot V. and S. A. Orszag, 1986. Renormalization group analysis of turbulence: 1. basic theory. J. Sci. Comput., 1, 1-51.